RSC Advances

REVIEW

View Article Online
View Journal | View Issue

Cite this: *RSC Adv.*, 2025, **15**, 2874

Asymmetric photoreactions catalyzed by chiral ketones

Bao-Ji Bian,[ab] Liu Yang,[b] Li-Xin Qiao,[b] Qiang Zhang *[a] and Wei He *[ab]

Asymmetric catalytic reactions are essential for synthesizing chiral drugs and fine chemicals, with their stereoselectivity influenced significantly by interactions between catalysts and substrates. Ketone catalysts have garnered considerable attention in the realm of asymmetric photoreactions because of their highly controllable structures, ease of availability, and environmental friendliness. This review highlights the application of various reported ketone catalysts in a range of asymmetric photoreactions, including [2 + 2] photocycloaddition, photoderacemization, photochemical rearrangement, asymmetric electrophilic amination, and asymmetric alkylation of aldehydes. This review discusses the design concepts, catalytic mechanisms, as well as the advantages and limitations of these catalysts within each reaction. The aim is to provide valuable insights for developing more effective asymmetric catalytic systems.

Received 5th December 2024
Accepted 9th January 2025

DOI: 10.1039/d4ra08581g

rsc.li/rsc-advances

1. Introduction

Asymmetric catalytic reactions play an important role in modern synthetic organic chemistry. To achieve asymmetric catalytic reactions, designing chiral catalysts with high enantioselectivity and universality is crucial. Before the introduction of the concept of organic catalysis, ketone-based catalysts emerged as one of the earliest investigated types among small molecule catalysts. They garnered extensive attention because of their cost-effectiveness, ready availability, eco-friendliness, and remarkable structural controllability.[1–7] The carbonyl group of ketone catalysts can undergo oxidation to form dioxiranes that serve as mild and selective oxidants. Leveraging this characteristic, in conjunction with precise spatial structure regulation, ketone catalysts find extensive applications in the asymmetric epoxidation of olefins. Dioxiranes in these catalysts have two directions for oxygen transfer when approaching olefins, both of which can be approached by olefins. Rationally designing the structure of a catalyst to control the reaction's direction with regard to the substrate is a challenge in studying this type of reaction. The design of catalysts in asymmetric epoxidation using the oxidizability of ketone catalysts has been covered in detail in numerous high-quality reviews.[8–12] These studies primarily focused on the period prior to 2015; therefore, this review does not delve into a detailed discussion on research pertaining to ketone catalysts in asymmetric epoxidation. Additionally, among the ketone catalysts used in asymmetric epoxidation reactions, the sugar-derived ketones developed by Shi's research group are the most widely used.[13] This type of catalyst has been successfully used in the synthesis of more than 20 key drug intermediates, such as KRAS G12C inhibitors, pradilolide A, and aplysiasecosterols A. As of August 2024, the relevant literature continues to increase annually and has a wide range of application values.[14–38] In addition, Tan *et al.* recently reported a ketone-catalyzed reaction for the enantioselective oxidation of N atoms that can be applied effectively to the enantioselective kinetic resolution of QUINAPO and related compounds.[39] The two highly enantiomeric QUINAPO *N*-oxide products can be converted easily to QUINAP without losing chiral integrity (Scheme 1). This is the first report of chiral ketone catalysts for the enantioselective oxidation of N atoms, and it is anticipated that there will be significant prospects for future research.

In addition to utilizing the oxidation characteristics of the ketone structure for designing ketone catalysts in catalytic reactions, ketone compounds can undergo n_p–π^* and π–π^*

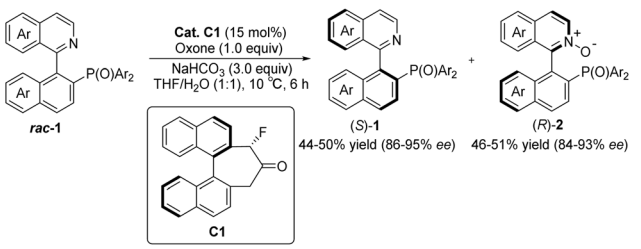

Scheme 1 Enantioselective oxidation of N atoms catalyzed by ketone C1.

[a]*Shaanxi Province Key Laboratory of Catalytic, School of Chemical and Environmental Science, Shaanxi University of Technology, Hanzhong 723001, P. R. China. E-mail: zhangqiang22@126.com*

[b]*Department of Chemistry, School of Pharmacy, Air Force Medical University, Xi'an 710032, P. R. China. E-mail: weihechem@fmmu.edu.cn*

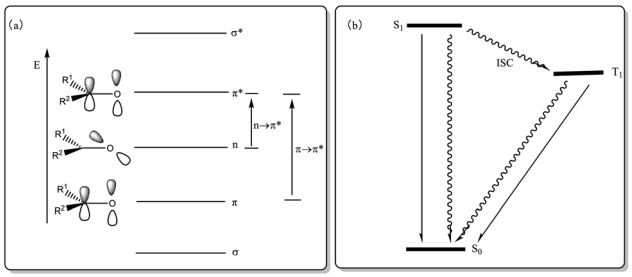

Fig. 1 (a) Electronic energy level and electronic transition of carbonyl group; (b) ISC process diagram of S_1 and T_1.

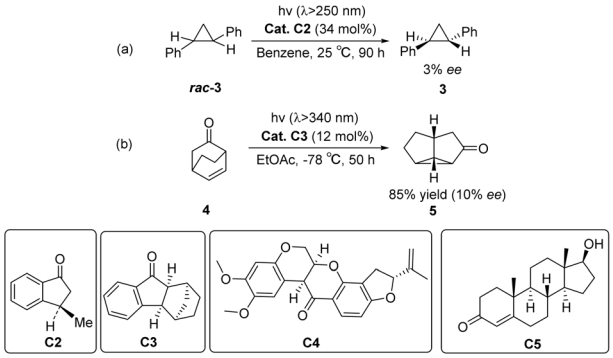

Scheme 2 Early exploration of chiral aromatic ketones as sensitizers in photocatalytic reactions.

transitions because their oxygen atoms have two pairs of lone electrons in nonbonding orbitals (occupying two nondegenerate orbitals, n_p and n_{sp}, respectively). The intersystem crossing (ISC) process can occur in S_1 (n_p, π^*) and T_1 (π, π^*), making it possible to utilize their optical properties for designing photosensitizers (PSs) that catalyze photochemical reactions (Fig. 1). The direct excitation of photoreactions with low absorption coefficients *via* light absorption is challenging, as it may lead to competitive processes and unnecessary side reactions; however, using a sensitizer allows for absorbing light and subsequently transferring excitation energy to the substrate at a lower level, thus enhancing chemical selectivity. Hence, the sensitization method offers distinct advantages. Sensitization is a classic mode of photocatalysis, with triplet sensitization being the most commonly used in organic synthesis. Triplet PSs are compounds that can be effectively excited to the triplet excited state and act as catalysts in photochemical reactions. A triplet PS meeting these conditions should exhibit the following characteristics: (1) strong absorption of excitation light; (2) higher energy than the receptor; (3) high-yield ISC for efficiently producing triplet states; (4) long triplet lifetimes to complete energy transfer.[40,41] The organic ketone molecule acts as a photocatalyst, absorbing energy and transitioning to S_1. Through the ISC process, S_1 is converted to T_1. At this point, the PS in the T_1 state interacts with the substrate, providing energy for the substrate to undergo a π–π^* transition while the ketone PS returns to its original state (S_0) to complete the catalytic cycle (Fig. 1). Compared with aliphatic ketones,[42] aromatic ketones have picosecond ISC, while alkyl ketones have nanosecond ISC, which means that most ketone PSs are aromatic.

In 1973, Ouannès *et al.* pioneered the utilization of the triplet sensitizer (*R*)-(−)-3-methyl-1-indanone **C2** to catalyze the enantioselective isomerization of a substrate. The earliest example involves the conversion of racemic *trans*-diphenylcyclopropane ***rac*-3** (DPC) into *cis*-DPC **3**, albeit with a modest ee value of only 3% (Scheme 2(a)).[43] The reason for the enantioselectivity may be due to the kinetic difference between the two enantiomers of racemic DPC during the energy transfer process from the triplet state. In 1980, Demuth *et al.* carried out photorearrangement of β,γ-unsaturated ketone **4** by chiral indanone sensitizer **C3**, and the yield of the isolated product **5** was 80–90%, and the ee value was 10% (Scheme 2(b)).[44] Subsequently, Rau *et al.* subjected the racemic mixture of optically active *trans*-3,5-diphenylpyrazoline to photolysis using (−)-rotenone **C4** and (+)-testosterone **C5** as sensitizers (Scheme 2). In comparison with the direct photolysis of diphenylpyrazoline under circularly polarized light, rotenone sensitization resulted in a 150% increase in reaction asymmetry; however, it still failed to provide effective enantioselectivity.[45] The reported PSs in the early stage exhibit sufficient ISC rates for substrate sensitization and reaction initiation; however, the resulting enantioselectivity remains significantly low. This could potentially be attributable to the rapid dissociation of the sensitizer–substrate complex upon excitation, thus hindering the well-defined chiral environment necessary for subsequent reactions. At the beginning of the 21st century, Bach designed aromatic ketone-type photocatalysts for asymmetric [2 + 2] photocycloaddition reactions[46] and photoderacemization reactions.[47] The application of ketones as PSs in the field of asymmetric photocatalysis has ushered in new developments. Currently, ketone-type asymmetric photocatalysts are mainly classified into three categories: diphenyl ketone-type photocatalysts, xanthone-type photocatalysts, and thioxanthone-type photocatalysts. These ketone catalysts have been widely applied in various asymmetric reactions, including asymmetric [2 + 2] photodimerization, photodecarboxylation, asymmetric electrophilic amination, asymmetric hydroxylation, and asymmetric alkylation of aldehydes. Although there are several reviews on asymmetric photocatalytic reactions in the literature,[48,49] this article specifically focuses on the design strategies for ketone-type catalysts used in these reactions. The synergistic effects between the PS unit and the chiral control unit are explored, providing insights into how the optimization of the design of these two components can significantly enhance the efficiency and selectivity of asymmetric photocatalytic reactions. Notably, this specific aspect of design strategies for ketone catalysts in asymmetric photochemical reactions has not been discussed in depth in the existing literature. Therefore, we contend that our review offers a valuable contribution to the current body of knowledge, providing new perspectives for developing catalysts in asymmetric light reactions. Additionally, Table 1 provides a summary of the types of reactions and substrates that are compatible with various

Table 1 Types and effects of photoreactions catalyzed by chiral ketones

Cat.	Reaction type	λ (nm)	Substrate characteristics	Example	ee (%)	Yield (%)	Ref.
C1	Kinetic resolution	—	QUINAPO	18	44–50	86–95	13
C2	Asymmetric isomerization reaction	>250	Indanones	1	3	—	43
C3	Asymmetric photorearrangement reaction	>340	Unsaturated ketones	2	10–13	80–90	44
C4–C5	Asymmetric photolysis reaction	315	*Trans*-3,5-diphenylpyrazoline	2	<5	—	45
C6	Intramolecular [2 + 2] photocycloaddition reaction	>310	Olefins and enones	1	19	100	50
C7		>300	α-Aminoalkyl and ketene	1	70	64	46
***ent*-C7**	Photoderacemization reaction	366	5-Substituted 3-phenylimidazolidine-2,4-dione	27	81–99	69–99	51
			3-Substitution indolone	13	79–99	83–96	52
C8	Intramolecular [2 + 2] photocycloaddition reaction	366	2-Quinolone and intramolecular double bond	6	6–90	21–75	53
	Asymmetric photorearrangement reaction	366	Spirooxindole epoxide	8	16–33	85–98	54
	Photoderacemization reaction	366	Benzothiazinone-1-oxide	5	20–55	52–95	55
***ent*-C8**	Intermolecular [2 + 2] photocycloaddition reaction	>366	2-Pyridone and acetylene dicarboxylate	12	59–92	40–88	56
C9	Intramolecular [2 + 2] photocycloaddition reaction	420	Quinolones and double bonds	18	87–99	79–99	57,58
	Intermolecular [2 + 2] photocycloaddition reaction	419	Quinolones and electron – deficient olefins	12	80–95	44–94	59
	Photoderacemization reaction	420	Racemic alkylidenecyclobutane and alkylidenecyclopentane	16	81–96	51–99	60
	Di-π-methane rearrangement reaction	420	Substituted quinolone	9	32–55	88–96	61
***ent*-C9**	Intermolecular Paternò–Büchi reaction	420	Quinoxalinones and olefins	13	86–98	50–99	62
	Photoderacemization reaction	420	Racemic 3-(1′-vinylidene)piperidin-2-one	17	89–97	52–99	63
		420	3-(1′-Alkenylmethylene)pyrrolidin-2-one	13	86–98	60–96	64
		420	Acrylamide	19	70–93	74–99	65
C10	Photocyclization	419	2-(4-Bromophenoxy)-3,5,5-trimethylcyclohex-2-enone	1	12	26	66
C11	Intermolecular [2 + 2] photocycloaddition reaction	437	β-Carboxyl substituted cycloenones and alkenes	5	46–85	26–61	67
		459	*N*,*O*-Acetals and olefins	10	83–95	54–93	68
C12	Intramolecular [2 + 2] photocycloaddition reaction	405	Quinolones and olefins	3	91–97	88–95	69
	Intermolecular [2 + 2] photocycloaddition reaction			4	73–98	24–99	
C13	Intermolecular [2 + 2] photocycloaddition reaction	393	Quinoxalinone and styrene	8	75–95	46–90	70
C14	Asymmetric electrophilic amination reaction	420–510	Diazene and enamine	15	91–99	30–95	71
C15		405	Alkenylcarbamate	5	95–99	53–66	72
C16	Asymmetric alkylation reaction	>400	Aldehyde	13	84–99	55–99	73
C17	Asymmetric α-hydroxylation reaction	>400	β-Ketoesters and β-ketoamides	21	85–95	78–98	74

catalysts, along with their corresponding enantiomeric excess (ee) values and yields.

2. Benzophenone-type photocatalysts

Early exploration of photocatalytic reactions using chiral aromatic ketones as sensitizers has shown promising yields;[44] however, the ee values remain relatively low. This could be attributable to the rapid dissociation of the sensitizer from the excited substrate after sensitization, leading to inadequate control over stereoselectivity and resulting in near-zero or very low enantioselectivity; therefore, controlling the reaction direction of the substrate to increase the ee value is crucial for achieving efficient asymmetric photocatalytic reactions. This goal can be achieved by introducing a chiral control unit into the structure of the PS, thus effectively regulating the selectivity of the PS regarding the substrate reaction direction when transmitting energy. Benzophenone was initially applied to this concept because of its good light absorption ability and potential to decompose into free radicals under light conditions, allowing it to exhibit a variety of roles in different light reactions.

2.1 Asymmetric [2 + 2] photocycloaddition reactions

The asymmetric [2 + 2] photocycloaddition reaction is a crucial strategy for constructing optically active cyclobutane fragments found in natural products. In 2003, Krische developed a [2 + 2] asymmetric cycloaddition reaction catalyzed by ketone **C6**; however, the ee value was only 19% (Scheme 3).[50] The reaction mechanism is shown in Fig. 2. Catalyst **C6** and quinolone **6** form complex **I**. Due to the distance dependence of energy transfer, the cycloaddition reaction only occurs on the **I** complex to control the formation of chirality and produce the **II** complex. Finally, the cycloadduct 7 dissociates, and ketone **C6** is regenerated to complete the catalytic cycle. The catalyst consists of two parts. The diphenyl ketone part is used as a sensitizing unit to transfer energy to the substrate to promote the reaction, and the other part has many N atoms that drive the substrate to form hydrogen bonds and control the spatial position of the substrate; however, the ee value obtained by the authors is not high, which may be due to the fact that the interaction between the single enantiomers of the catalyst and the substrate does not have the advantage of photoreaction kinetics. Benzophenone has a low triplet state energy and a short absorption wavelength that can lead to low sensitization efficiency.

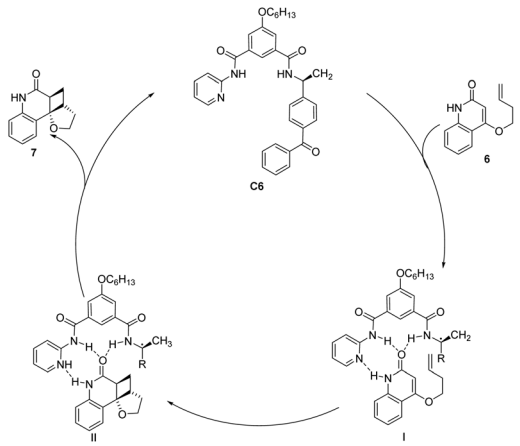

Fig. 2 Mechanism of asymmetric photo [2 + 2] cycloaddition of ketone **C6** to quinolone.

Furthermore, before the cyclization step of the sensitized substrate is completed, the catalyst separates from the reactant, resulting in most of the substrate not being in a chiral environment, thus reducing the enantiomeric selectivity of the products.

In 2005, Bach designed ketone **C7** for the asymmetric catalytic conjugate addition of α-aminoalkyl and ketene and achieved a significant breakthrough in the field of asymmetric photocatalysis.[46] A chiral spirocyclic pyrrolizidine compound was synthesized through the utilization of a 30 mol% catalyst **C7** for substrate catalysis. The resulting yield was determined to be 64%, accompanied by an ee value of 70% (Scheme 4). The catalyst's design concept bears a resemblance to that proposed by Krische.[50] By utilizing hydrogen bonding, the substrate's spatial position is immobilized, thus establishing a chiral environment. Subsequently, introducing an aromatic ketone sensitizer endows the catalyst with the capability to facilitate energy or electron transfer. This mechanism is visually depicted in Fig. 3.[34] The catalyst controls the spatial position through hydrogen bonds (shown as "a" in Fig. 3), and when activated by light, the benzophenone group accepts an electron from the N atom in a pyrrolidine (shown as "b" path in Fig. 3). The transfer of electron-deficient nitrogen ortho-hydrogen protons to benzophenone radical anions (shown as the "c" path in Fig. 3) and the remaining free radicals undergo intramolecular cyclization. The hydrogen initially transferred to benzophenone is returned to the carbon radical of the product

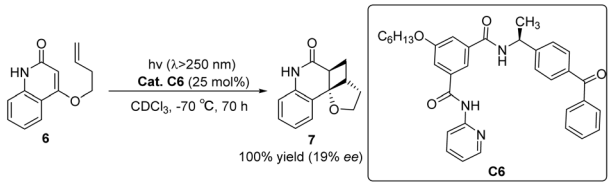

Scheme 3 Ketone **C6** catalyzed asymmetric [2 + 2] photocycloaddition of ketenes.

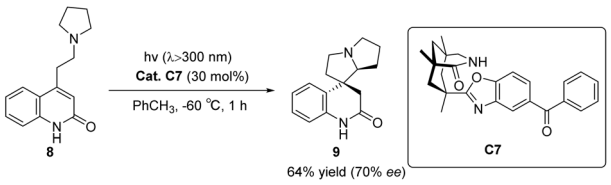

Scheme 4 Ketone **C7** catalyzed asymmetric conjugate addition of α-aminoalkyl to ketenes.

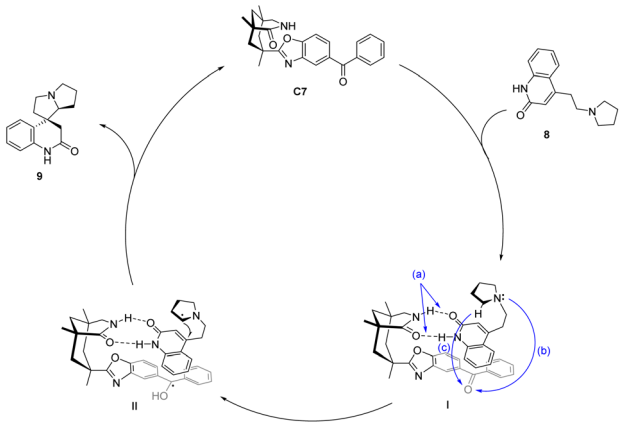

Fig. 3 Mechanism of asymmetric conjugate addition of α-aminoalkyl and ketene catalyzed by xanthone C7.

to complete the reaction cycle. Ketone **C7** not only promotes the required enantiomeric differentiation but also acts as a photooxidant.

2.2 Photoderacemization reactions

The deracemization reaction pertains to the transformation in which the quantity of one enantiomer is augmented while the quantity of the other enantiomer is diminished, resulting in the conversion of a racemic mixture into a nonracemic form.[75] This process involves reducing the entropy, necessitating energy expenditure. Thermodynamic approaches are incapable of transforming racemates into enantiomers under equilibrium conditions; however, the photochemical deracemization reaction effectively surmounts the kinetic obstacles and thermodynamic difficulties encountered in chemical conversion. Through this reaction, the racemic compound is converted directly into its enantiomer, resulting in the acquisition of a singular chiral compound while compensating for the entropy loss incurred during the energy compensation process. Additionally, optical racemization exhibits a 100% atomic efficiency, surpassing the traditional resolution process, which can only achieve a maximum enantiomeric yield of 50%, resulting in a wastage of 50% of the enantiomer. Hence, it possesses distinct advantages compared with conventional kinetic resolution (Fig. 4).

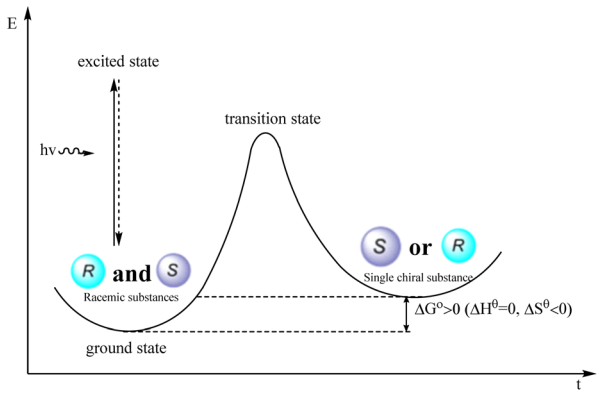

Fig. 4 Thermodynamic process of photocatalytic deracemization reaction.

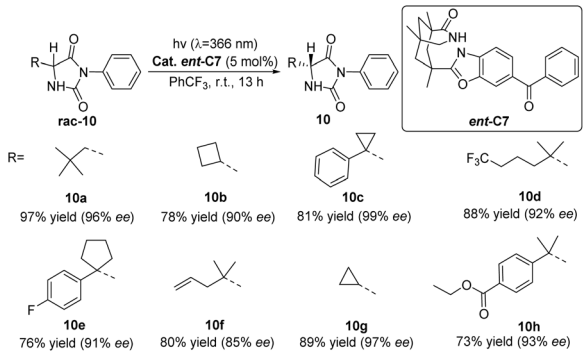

Scheme 5 The photochemical deracemization of 5-substituted 3-phenylimidazolidine-2,4-dione (hydantoin) catalyzed by ***ent*-C7**.

In 2021, Bach proposed a new photochemical deracemization method based on the selective hydrogen atom transfer (HAT) of photocatalysts. Using the chiral diarylketone photocatalyst ***ent*-C7** to catalyze the photoderacemization of ***rac*-10** (Scheme 5),[51] it should be noted that the reaction occurs through selective HAT rather than *ent*. From this principle, it is not difficult to find that other compounds with two hydrogen bonding sites may also be deracemized by the catalyst ***ent*-C7**, and its application range needs to be further explored.

Bach provided a more detailed elucidation in 2023 on the racemization mechanism of chiral imidazolidine-2,4-dione (hydantoin) catalyzed by chiral benzophenone ***ent*-C7**.[76] Furthermore, they once again confirmed that the catalytic cycle is achieved through reversible HAT. The catalyst was confirmed to bind two enantiomers through two hydrogen bonds using nuclear magnetic resonance titration. Specifically, **I** forms a ground state conformation through these hydrogen bonds. The distance between the carbonyl oxygen atom and the hydrogen atom in the stereocenter is very close, leading to HAT upon excitation. Subsequently, under photoexcitation, benzophenone extracts the hydrogen atom from the sp^3 hybrid carbon center, resulting in the breaking of the C–H bond *via* a nonlinear transition state to form an achiral radical known as **II**. Enol intermediate **III** is generated by back HAT, followed by a tautomerization reaction that produces two enantiomers; however, only **10** returns to the catalytic cycle while ***ent*-10** is depleted continuously. As a result, enantiomer **10** becomes increasingly enriched. In complex **IV**, the hydrogen atom is positioned on the opposite side of the 3-phenylimidazolidine-2,4-dione ring, an inaccessible location (Fig. 5). The keto radical intermediate was identified through transient absorption spectroscopy, and it was further confirmed that HAT exclusively occurred on a single enantiomer, thus precluding the aforementioned process. Consequently, this led to the accumulation of **10** chiral compounds.

Subsequently, Bach reported that catalyst ***ent*-C7** (10 mol%) could catalyze the deracemization of racemic 3-substituted oxindoles (Scheme 6),[52] which occurred through reversible HAT

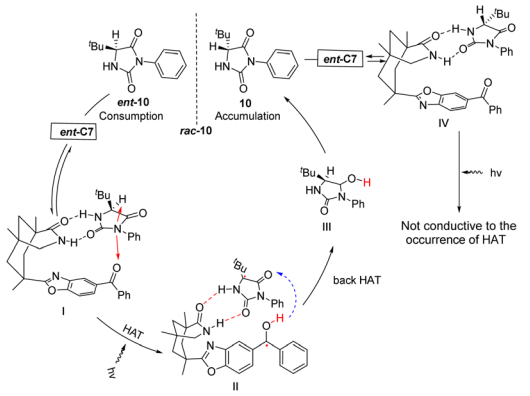

Fig. 5 Mechanism of deracemization of ***rac*-10** catalyzed by ketone ***ent*-C7**.

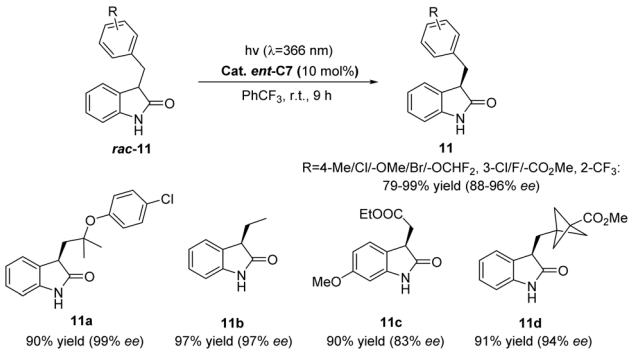

Scheme 6 Deracemization of racemic 3-substituted oxindoles catalyzed by ***ent*-C7**.

in the substrate–catalyst complex. In addition, this method is characterized by its ability to predictably edit the chiral center at the C3 position of racemic 3-substituted oxindoles (***rac*-11**), and the light energy compensates for the related entropy loss, which has important theoretical and application value for drug synthesis that requires controllable editing of a chiral center.

3. Xanthone-type photocatalysts

Although benzophenone possesses the basic characteristics of a PS, its relatively low triplet state energy limits its catalytic performance as a photocatalyst, resulting in low catalytic efficiency and selectivity; therefore, optimizing its structure to design photocatalysts with better photochemical reactivity and enantioselectivity has become a key area of focus.

3.1 Asymmetric [2 + 2] photocycloaddition reactions

Considering that both ketone **C7** and ketone **C6** are diphenyl ketone derivatives, is it plausible to assume that ketone **C7** can also catalyze the intramolecular asymmetric [2 + 2] photocycloaddition reaction, similar to ketone **C6**. A study conducted by Bach revealed that the reaction rate facilitated by ketone **C7** is superior to that facilitated by ketone **C6**, albeit the

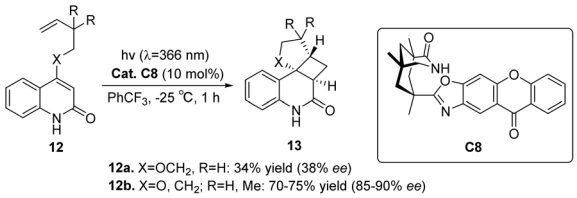

Scheme 7 Asymmetric intramolecular [2 + 2] photocycloaddition of 2-quinolone substrates catalyzed by 2-quinolone **C8**.

enantioselectivity remains considerably low. This can be attributed to the relatively low triplet energy and short wavelength absorption of benzophenone **C7**, resulting in poor enantioselectivity (39% ee). Consequently, the catalyst structure was optimized to design a xanthone-type catalyst **C8**. The bicyclic lactam unit structure in ketone **C8** can be pre-combined with the substrate to ensure that the sensitizing part is close to the substrate chromophore. The xanthone catalyst **C8** exhibits a significantly elevated absorption coefficient at a wavelength exceeding 350 nm ($\varepsilon_{350} = 9200$ in $PhCF_3$). Moreover, a substantial degree of enantioselectivity can be achieved with a mere 5–10 mol% of catalyst **C8** (Scheme 7).[53,77]

The enantioselectivity observed in the intramolecular [2 + 2] photocycloaddition reaction is contingent upon the extent of substrate–catalyst association mediated by hydrogen bonding (step 1, Fig. 6), the partial effective sensitization of xanthones (step 2, Fig. 6), and the subsequent rate of cyclization (step 3, Fig. 6). The association behavior of the substrate quinolone compounds with the catalyst was studied using NMR titration experiments.[78] It was discovered that the catalyst was fully associated with the substrate prior to the initiation of the reaction. The increase in enantioselectivity for **C7** and **C8** is determined by the efficiency of sensitization and the subsequent cyclization rate. The disparity in enantioselectivity between substrates quinolone **12a** and quinolone **12b** (X = O, R = H) in Scheme 7 arises from the dissociation of the substrate

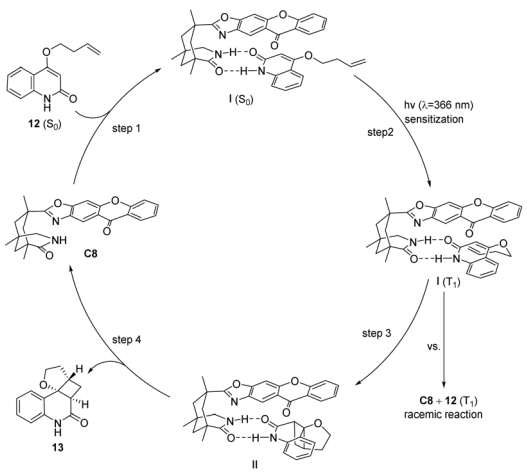

Fig. 6 Mechanism of asymmetric [2 + 2] photocycloaddition of quinolones catalyzed by ketone **C8**.

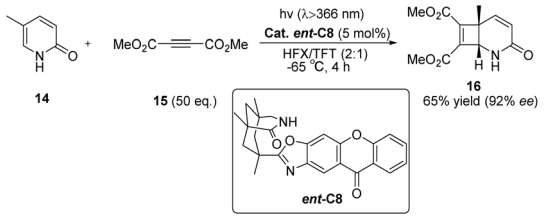

Scheme 8 Intermolecular [2 + 2] asymmetric photocycloaddition between 2-pyridone and acetylene dicarboxylate catalyzed by ***ent*-C8**.

from the catalyst prior to photocycloaddition, resulting in a reduction in enantioselectivity.

Subsequently, Bach also reported the intermolecular [2 + 2] photocycloaddition reaction between 2-pyridone and acetylene dicarboxylate catalyzed by ***ent*-C8** that can achieve high enantioselectivity (Scheme 8).[56] These excellent outcomes were achieved as a result of the following factors: (1) the rapid addition of alkynes to the excited substrate, (2) the effective binding of the substrate to the catalyst through hydrogen bonds, and (3) the high enantiomeric differentiation ensured by the 1,5,7-trimethyl-3-azabicyclo[3.3.1]nonane-2-one scaffold.[79]

Comparing the structures of the two PS components, xanthone **C8** and benzophenone **C7**, it can be observed that the triplet energy of xanthone **C8** is higher than that of benzophenone **C7**. Additionally, since the shape of the chromophore is approximately planar in the excited state, it facilitates closer proximity for energy transfer with the substrate. In contrast, the photochemically excited diphenyl ketone is not planar, resulting in a faster dissociation rate of the substrate during the reaction, leading to a decrease in the ee value. It can be seen that for the [2 + 2] photocycloaddition reaction, the photocatalyst of xanthone type **C8** has more advantages than the photocatalyst of benzophenone type **C7**.

3.2 Other asymmetric photocatalytic reactions

Xanthone-type photocatalysts, in addition to their application in asymmetric [2 + 2] photocycloaddition reactions, have also been utilized in various other reactions, such as asymmetric photorearrangement reactions and photoderacemization reactions.

Inspired by the application of benzophenone in the rearrangement reaction of spirophenol indole epoxides reported by Zhang *et al.*,[80] Bach used xanthone **C8** to study the photochemical rearrangement of spirooxindole epoxides (Scheme 9).[54] At $\lambda =$ 366 nm, the yield of spirooxindole ***rac*-17** rearranged to 3-acyl-3-alkylindole-2-one **18** can reach 92–98%, and the ee value is 20–33%. The low enantioselectivity may be due to the relatively slow

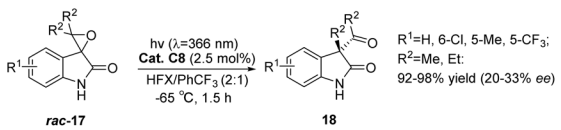

Scheme 9 Xanthone **C8** catalyzes the photochemical rearrangement of spirooxindole epoxides (HFX = hexafluoro-*m*-xylene).

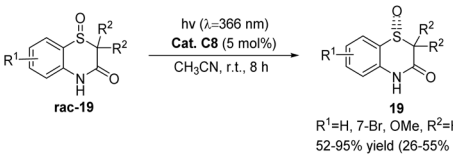

Scheme 10 Deracemization reaction of benzothiazinone-1-oxide catalyzed by ketone **C8**.

rearrangement steps after sensitization that generate intermediates. Additionally, most intermediates undergo rearrangement after dissociation from the chiral catalyst, resulting in low ee values. This provides a new example for applying bifunctional ketone catalysts in other asymmetric photocatalytic reactions, further proving the universality of this type of catalyst.

Ketone **C8** also exhibits catalytic activity in the deracemization reaction of racemic benzothiazinone-1-oxide. Despite a high substrate conversion rate, the resulting product's ee value is significantly low (Scheme 10).[55] This could potentially be attributable to the instability of the catalyst xanthone employed in this reaction.

From the above discussion, it is clear that the appropriate choice of excitation wavelength, along with the absorption characteristics of the substrate and the corresponding substrate–photocatalyst complex, influences the reaction significantly. The triplet energy of the PS must be higher than the triplet energy of the substrate so rapid energy transfer can occur even at low temperatures. Additionally, if excitation can occur in the absence of a photocatalyst, the enantioselectivity will be compromised because of background reactions. The oxoxanthone photocatalyst ***ent*-C8** possesses a significantly higher extinction coefficient compared with the substrate and effectively absorbs nearly all photons. Consequently, the racemic background reaction is attenuated, leading to enhanced enantioselectivity. Conversely, benzophenone derivative **C7** exhibits a much lower extinction coefficient at 366 nm that inadequately weakens the competing racemic background reaction, resulting in reduced selectivity. Henceforth, it is crucial to design photosensitive units based on reaction characteristics rationally.

4. Thioxanthone photocatalysts

Common chromophores, such as carbonyl compounds, ketenes, and aromatic hydrocarbons, require a wavelength region of λ = 250–350 nm for direct excitation. Medium-pressure mercury lamps are commonly used as light sources for this purpose. Nevertheless, advancing scientific research often relies on employing uncomplicated techniques to achieve intended outcomes. Is employing visible light as an illuminating source to successfully catalyze the reaction feasible? The energy associated with a photon of wavelength λ = 400 nm is approximately 300 kJ mol^{-1}, surpassing the triplet energy of numerous photochemical substrates. This observation suggests the feasibility of the proposed concept. Furthermore, the irradiation of xanthones in toluene at a wavelength of 366 nm

results in swift decomposition, with a duration of less than 10 minutes. Xanthones are stimulated by ultraviolet light wavelengths, and the higher energy of these shorter wavelengths may directly excite the substrate, leading to undesired side reactions. The utilization of a suitable sensitizer and the substitution of ultraviolet light with visible light for exciting photoreactions are evident strategies that significantly enhance experimental convenience and reaction selectivity.

4.1 Asymmetric [2 + 2] photocycloaddition reactions

In 2014, Bach devised a novel chiral thioxanthone **C9** (Scheme 11) capable of facilitating the intramolecular [2 + 2] asymmetric cycloaddition reaction through absorbing visible light, employing a mere 10 mol% of ketone **C9**.[57] The resulting ee reaches an impressive 92%, while the attained yield is 86%. This reaction maintains a high degree of enantioselectivity even under ambient conditions. Furthermore, the author employed an alternative set of lamps (RPR-4190 Å) that do not emit ultraviolet light in order to address the small emission of ultraviolet light from the visible light source utilized. By conducting the experiment under identical conditions as previously mentioned, the substrate was obtained with a yield of 84% and an ee of 96%.

The intramolecular [2 + 2] photocycloaddition transition state of the thioxanthone-type catalyst is similar to that of the xanthone-type catalyst (Fig. 7). The differentiation of enantiomers is provided by the planar xanthone through hydrogen bonds, and the energy from absorbed photons is transferred to quinolone by triple energy transfer; therefore, the attack on the quinolone double bond occurs with high selectivity.

The known asymmetric [2 + 2] photocycloaddition reactions are all applied to substrates without alkyl substituents at the α-position because the substituents at this position may damage

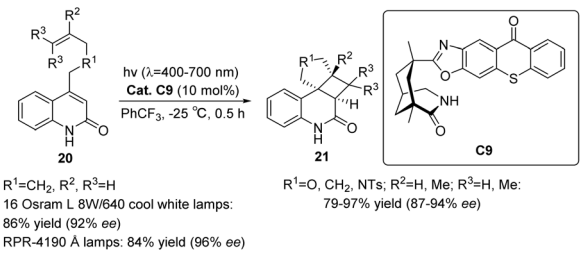

Scheme 11 Ketone C9 catalyzed intramolecular [2 + 2] asymmetric photocycloaddition reaction.

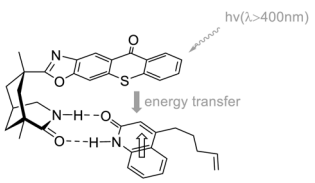

Fig. 7 Transition state model for sensitization and enantioface differentiation in the coordination complex of catalyst C9 and quinolone.

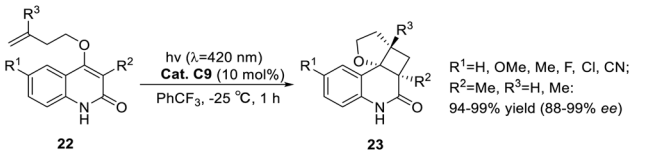

Scheme 12 Ketone C9 catalyzed intramolecular [2 + 2] asymmetric photocycloaddition of 3-alkyl substituted quinolones.

the coordination of the carbonyl group from a structural point of view. In 2020, Bach posed a challenge to the synthesis of cyclobutanes with a high degree of substitution.[58] Surprisingly, compared with unsubstituted quinolones, the alkyl substituents at the α-position of the carbonyl group not only did not block the binding to the catalyst but also resulted in a significant decrease in triplet energy ($\Delta_{ET} \approx 25$ kJ mol^{-1}), which produced a beneficial effect. The intramolecular asymmetric [2 + 2] photocycloaddition of 3-alkylquinolone catalyzed by ketone **C9** can be obtained in good yields and ee values (Scheme 12).

In comparison with xanthone compounds, thioxanthone compounds exhibit a red shift in their maximum absorption wavelength ($\lambda_{max} = 390$ nm).[81] Furthermore, thioxanthone **C9** demonstrates a detectable lifetime at $\lambda = 400$–700 nm, suggesting its suitability for facilitating photochemical reactions when exposed to visible light sources. The intermolecular [2 + 2] asymmetric photocycloaddition reaction of quinolone compounds with electron-deficient olefins was catalyzed by chiral thioxanthone **C9** (10 mol%).[59] The resulting cyclobutane product exhibited an ee value of up to 95% (Scheme 13). An increase in the amount of coupling agent olefins in this reaction is associated with an increase in both the reaction rate and enantioselectivity. This phenomenon can be attributed to a higher proportion of cyclization occurring prior to catalyst dissociation, thus leading to enhanced enantioselectivity. Additionally, kinetic data indicate that the enantioselectivity is influenced by the sluggish reaction rate. It is postulated that other substrates featuring lactam binding motifs and exhibiting rapid intermolecular reaction rates would similarly be suitable for enantioselectively catalyzed intermolecular [2 + 2] photocycloaddition reactions.

In the presence of a chiral sensitizer ***ent*-C9** (10 mol%), 3-substituted quinoxalinones can engage in intramolecular or intermolecular asymmetric aza-Paternò–Büchi reactions with diverse aryl-substituted or chain olefins (Scheme 14), resulting in the formation of chiral azetidines.[62] When the C3 position of

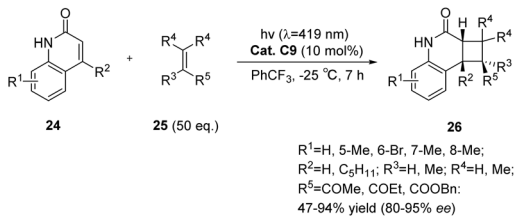

Scheme 13 Ketone C9 catalyzed intermolecular asymmetric [2 + 2] photocycloaddition reaction.

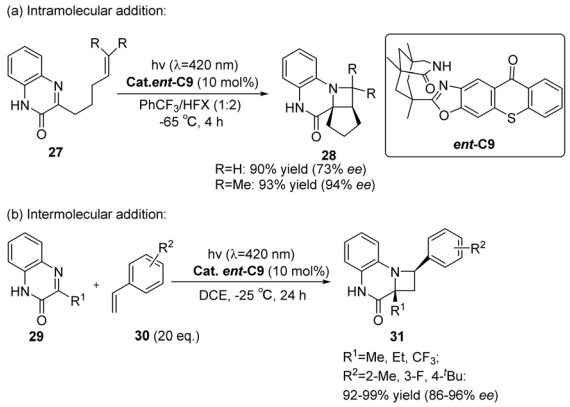

Scheme 14 Asymmetric [2 + 2] photocycloaddition of carbonyl-olefins catalyzed by ***ent*-C9** (HFX = hexafluoro-*m*-xylene).

the quinolone (**27** or **29**) is not replaced, this reaction does not produce azamine (**28** or **31**), indicating that the reaction mode of quinoxalinone is largely dependent on the 3-substituent, and the 3-substituent plays an important role in a certain intermediate process.

For the intermolecular [2 + 2] cycloaddition transition state, as shown in Fig. 8, the *Si* face of **29** is shielded by thioxanthone so that styrene only attacks the *Re* face. The intermediate 1,4-diradical **II** collapses after the ISC process to form the azetidine product **31**. Although the triplet energy transfer from ***ent*-C9** to styrene is energetically feasible, this pathway is less likely because the enantioselectivity is so high when the catalyst loading is only 10 mol%, proving that ***ent*-C9** does not undergo triplet energy transfer to styrene.[62]

Catalysts primarily employ hydrogen bonding interactions with the substrate in their structure to regulate the direction of the reaction, utilizing the chiral control elements of the aforementioned PSs; however, the current hydrogen bond skeleton exhibits relatively limited diversity, and designing different hydrogen bond skeleton units is of great significance for expanding more substrates.

In 2017, Bach conducted a novel endeavor to advance the development of a hydrogen bond skeleton,[66] incorporating a thiourea group as a chiral control unit and devised a thiourea–thioxanthone compound **C10**. The findings indicated that ketone **C10** effectively facilitated the photocyclization of 2-(4-bromophenoxy)-3,5,5-trimethylcyclohex-2-enone **32** (Scheme 15). Although the yield and enantioselectivity of the product are relatively low, the catalyst's success lies in

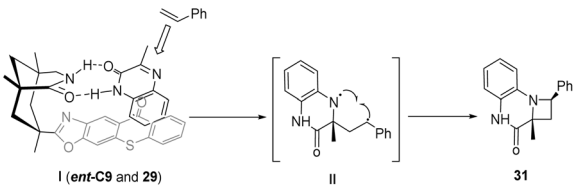

Fig. 8 Transition state analysis of intermolecular [2 + 2] photocycloaddition catalyzed by thioxanthone ***ent*-C9**.

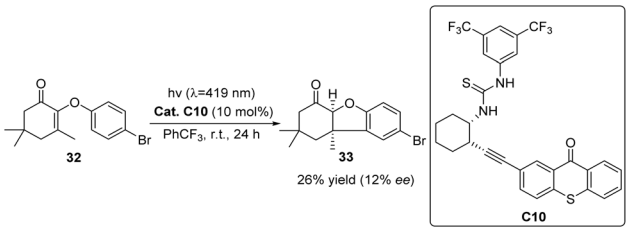

Scheme 15 Ketone **C10** catalyzed photocyclization reaction.

introducing a novel chiral hydrogen bond scaffold into the chiral control unit. The inclusion of thiourea on this scaffold enables the formation of two hydrogen bond sites, thus expanding the scope of existing bifunctional catalysts and providing valuable insights for the future design of new chiral control units.

In 2020, Bach introduced chiral phosphoric acid (CPA) into asymmetric photochemical conversion for the first time and introduced two thioxanthone groups as PS units at the 3,3′-position of the BINOL skeleton to obtain a new CPA binding site catalyst **C11**.[67] CPA is a representative Brønsted acid in thermochemical reactions.[82] Here, its role is to generate a chiral environment and activate the substrate through hydrogen bonds during the conversion process. The catalyst effectively decreases the triplet energy of the substrate through hydrogen bonding, resulting in notable enantiomeric discrimination. It demonstrates high efficacy as a catalyst for the intermolecular [2 + 2] photocycloaddition reaction of β-carboxyl substituted cycloenones, with a 61% product yield with an 85% ee (Scheme 16).

The asymmetric [2 + 2] photocycloaddition of *N*,*O*-acetals with olefins can also be catalyzed by thioxanthone **C11** (10 mol%), resulting in yields ranging from 54% to 96% and ee values ranging from 84% to 98% (Scheme 17). The successful reaction relies on the triplet energy transfer of thioxanthone and the efficient enantiomeric differentiation of CPA.[68]

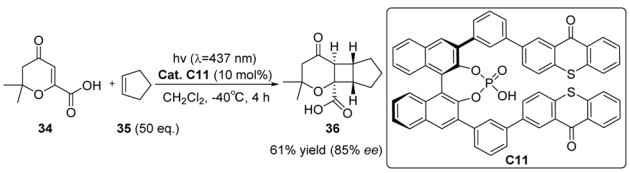

Scheme 16 Ketone **C11** catalyzed intermolecular [2 + 2] asymmetric photocycloaddition of β-carboxyl substituted cyclic ketenes.

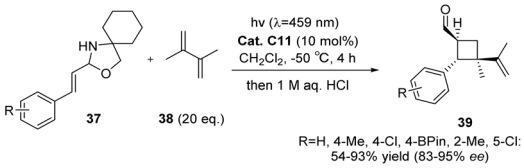

Scheme 17 The [2 + 2] asymmetric cycloaddition reaction of *N*,*O*-acetals with olefins catalyzed by **C11** was studied.

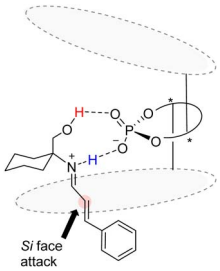

Fig. 9 Transition state model of asymmetric [2 + 2] cycloaddition catalyzed by catalyst **C11**.

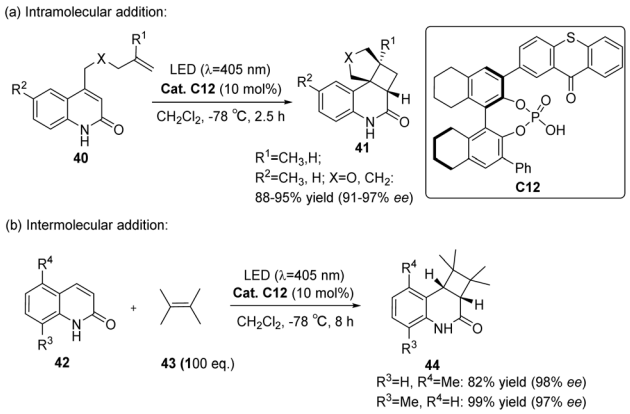

Scheme 18 Intramolecular and intermolecular photocycloaddition of quinolones catalyzed by ketone **C12**.

The Bach reaction is based on the prechiral imine ion addition model proposed by Akiyama *et al.*[83] An analogous transition state model for catalyst **C11** and substrate enantiomer differentiation is proposed, wherein the aryl group of the acid undergoes attack from the *Si* face (Fig. 9).

Takagi *et al.*[69] employed a C1 symmetric CPA as the main chiral chain. They introduced thioxanthone as a photosensitive component to synthesize catalyst **C12**. Subsequently, they conducted intramolecular and intermolecular [2 + 2] photocycloaddition reactions of quinolones, resulting in the attainment of higher ee values (91–98%) (Scheme 18). In photoconversion, the chiral environment is established through the complexation of phosphoric acid and quinolone. The

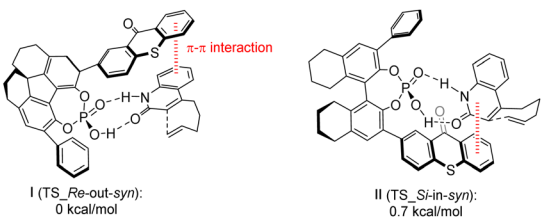

Fig. 10 Transition state energy calculation of ketone **C12** with the substrate (the schematic structure and relative Gibbs energy of each enantiomer at 195.15 K in the intramolecular [2 + 2] photocycloaddition reaction).

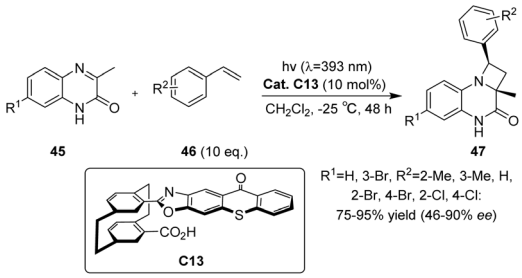

Scheme 19 Enantioselective Paternò–Büchi reaction catalyzed by ketone **C13**.

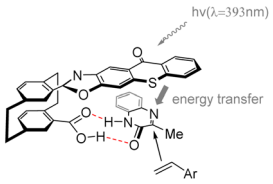

Fig. 11 Transition state model is proposed for the enantioselective Paternò–Büchi reaction catalyzed by ketone **C13**.

enantioselectivity is influenced significantly by the π–π interaction between the thioxanthone moiety of phosphoric acid and the substrate. The transition state with the lowest energy for each enantiomer in the reaction is depicted in Fig. 10. In both instances, the quinolones are oriented towards the thioxanthone ring on CPA. Notably, the main product obtained corresponds to the **I** transition state, thus confirming the experimental findings.

In 2023, Huo *et al.*[70] developed a novel photocatalyst **C13** based on thioxanthone, featuring a hamburger-shaped structure and planar chirality (Scheme 19). This catalyst was successfully employed in the enantioselective Paternò–Büchi reaction of quinoxalinone **45** and styrene **46** under visible light irradiation to afford azetidines. The catalyst **C13** and the substrate amide **45** establish a stabilized spatial position through hydrogen bonding interactions. Upon irradiation, the thiazolone group of the intermediate undergoes excitation, leading to intramolecular energy transfer to the substrate amide. Due to the spatial shielding provided by the thioxanthone group, styrene is unable to approach the *Si* face of the transition state model (Fig. 11).

Through the above content, it can be concluded that the successful use of ketone catalysts in asymmetric reactions depends on two basic factors: (a) including a sensitizing ketone unit for energy or electron transfer and (b) incorporating chiral control units that interact with the substrate to ensure effective enantiomer or group differentiation. The rate of substrate dissociation is slower than the enantioselectivity determination step of the reaction. Consequently, even after sensitization, the excited substrate still encounters the spatial bias imposed by the control element to ensure a distinct chiral environment.

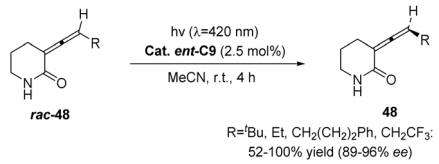

Scheme 20 Deracemization of 3-(1′-alkenyl)piperidin-2-ones catalyzed by ketone *ent*-C9.

4.2 Photoderacemization reactions

In 2018, Bach first reported the pioneering achievement of a successful photoderacemization reaction. By employing a catalytic amount (2.5 mol%) of the triple sensitizer ***ent*-C9**, various racemic 3-(1′-methylene)piperidin-2-ones were effectively transformed into their corresponding single enantiomers under visible light irradiation at a specific wavelength of 420 nm. The resulting yield exceeded 56%, while the ee value ranged from 89% to 97% (Scheme 20).[63] The sensitizer is transferred to allene *via* triplet energy transfer and subsequently separated based on the distinct energy transfer efficiencies of the two enantiomers.

The proximity between the sensitizer ***ent*-C9** chromophore and the allene double bond of substrate ***ent*-48** is closer compared with that of substrate **48**, resulting in a faster triplet energy transfer between ***ent*-48** and the sensitizer. The disparity in association constants (ground state thermodynamics) and sensitization efficiency (excited state kinetics) between **48** and ***ent*-48** with the catalyst leads to distinct total sensitization rates. Consequently, the intramolecular sensitization mechanism of **48** is unfavorable, enabling the accumulation of **48** (Fig. 12).[63]

Yuan *et al.* conducted a theoretical investigation using density functional theory (DFT).[84] Using the enantiomeric conversion of 3-(3,3-dimethyl-1-butyl-1-subunit)-2-piperidone from Scheme 20 as a case study (R = ^{t}Bu), they elucidated the mechanism underlying the deracemization reaction catalyzed by ***ent*-C9** (see Fig. 13). The PS ***ent*-C9** is excited under visible light ($\lambda = 420$ nm) irradiation ($S_0 \rightarrow S_2$) because of the potential surface crossing between the S_1 and S_2 states; therefore, a fast internal conversion ($S_2 \rightarrow S_1$) occurs near the intersection. At this time, the energy of the T_1 state is slightly lower than that of the S_1 state, and the PS undergoes ISC ($S_1 \rightarrow T_1$). The T_1 state of the PS ***ent*-C9** undergoes Dexter-type energy transfer to the S_0 state of ***ent*-48**, forming the S_0 state of the PS ***ent*-C9** and the T_1 state of ***ent*-48**. Finally, the T_1 state of ***ent*-48** can pass through the potential energy surface of the triplet state and transform into the transition state between ***ent*-48** and **48** of the ground

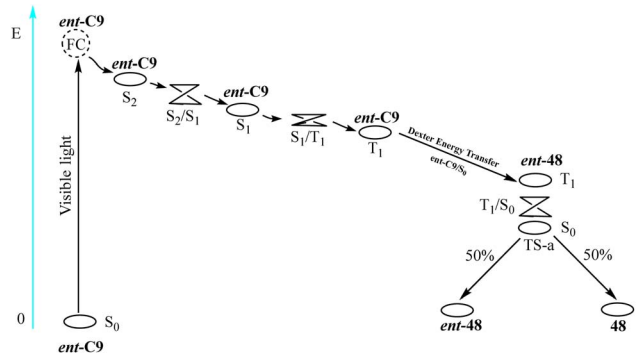

Fig. 13 Photosensitive deracemization mechanism of racemates.

state S_0. This transition state then forms a **48** : ***ent*-48** ratio of 1 : 1. The newly generated ***ent*-48** can be resensitized to form TS-a by catalyzing thioxanthone ***ent*-C9**, but **48** cannot. By repeating this process, the amount of ***ent*-48** is halved in each photocatalytic cycle, while the amount of **48** increases accordingly. The mechanism reveals that complete conversion of ***ent*-48** to **48** is unattainable, thus limiting the ee value infinitely close but not equal to 100%. From the theoretical calculation, deracemization occurs because limited occurrence of energy transfer within ***ent*-C9** and **48**, consistent with the spatial effects analysis results (Fig. 12). It can be observed that designing a new deracemization photocatalyst based on the disparity between the ground state association constant and excited state sensitization efficiency of two diastereomeric complexes proves to be an effective strategy.

In 2019, Bach reported that under irradiation with visible light (λ = 420 nm), ***rac*-49**, a 3-allyl-substituted quinolone, underwent a triple-sensitized di-π-methane rearrangement reaction to yield the corresponding ***rac*-50**, a 3-cyclopropyl quinolone. By employing chiral thioxanthone sensitizer **C9**, cyclopropane underwent a triple-sensitized deracemization reaction, forming enantiomerically pure 3-cyclopropylquinolone **50**. The yields ranged from 88% to 96%, while the ee values were between 44% and 55% (Scheme 21).[61]

In the subsequent year, Bach employed the chiral triplet sensitizer ***ent*-C9** (2.5 mol%) to facilitate the racemization reaction of ***rac*-51**, resulting in an enhanced ee value of 86–98% for product **51** (Scheme 22). The photocatalyst also operates through selective recognition of an olefin enantiomer and a hydrogen bond-mediated triplet sensitization process.[64]

Similarly, the chiral sensitizer thioxanthone ***ent*-C9** (2.5 mol%) is capable of catalyzing the photoderacemization of enamide ***rac*-52** at 420 nm. The resulting acrylamide **52** exhibits

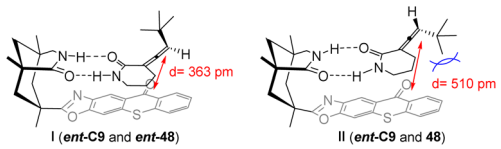

Fig. 12 The deracemization transition state model of 3-(1′-alkenyl) piperidin-2-one catalyzed by ***ent*-C9**.

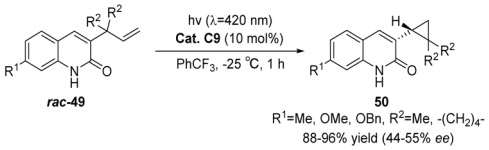

Scheme 21 Deracemization of 3-cyclopropylquinolone catalyzed by ketone **C9**.

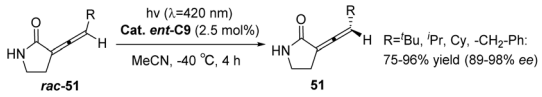

Scheme 22 Deracemization of ***rac*-49** catalyzed by ketone ***ent*-C9**.

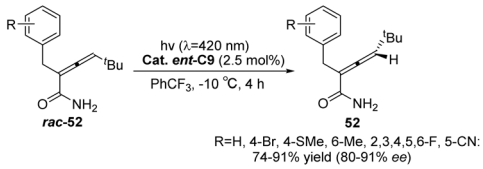

Scheme 23 Ketone ***ent*-C9** catalyzed photochemical deracemization of enamides.

an ee value ranging from 80% to 91% (Scheme 23).[65] In addition to the difference in the degree of association between the enantiomer and the catalyst caused by the hydrogen bonding between the catalyst and the substrate, it was also found *via* DFT calculations that this result was affected by the attractive dispersion interaction between the π system of the propylene and ketone catalyst. One of the enantiomers, the C–H or C–halogen bond, is perpendicular to the π system, forcing propylene away from the thioxanthone chromophore. In the case of another propylene enantiomer, the interaction between the C–H bond at the terminal carbon atom of propylene and the outer benzene ring of thioxanthone, known as the CH–π interaction, leads to propylene being in close proximity to the chromophore. Enantiomers in close proximity to the chromophore exhibit a higher reaction rate, ultimately resulting in the observed outcome (Fig. 14). This discovery represents the first instance in which a dispersion interaction has been identified as a valuable means to enhance the enantioselectivity of photochemical reactions, thus offering a novel approach for the future design of enantioselective photoinduced conversions.

In 2022, Bach reported a visible-light-mediated photocatalytic deracemization method for synthesizing axially chiral olefins. A variety of racemic alkylidenecyclobutanes ($n = 4$) and alkylidenecyclopentanes ($n = 5$) can be deracemized by triplet energy transfer with only 2 mol% chiral thioxanthone **C9**, achieving up to 81–96% ee (Scheme 24).[60]

In the presence of the catalysts ***ent*-C8** or ***ent*-C9**, the photoderacemization reaction of 3-spirocyclopropyl 2-oxindoles yields a high ee value (Scheme 25) and exhibits a broad

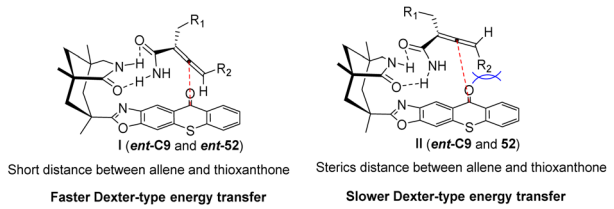

Fig. 14 Transition state model of deracemization of acrylamide by *ent*-C9.

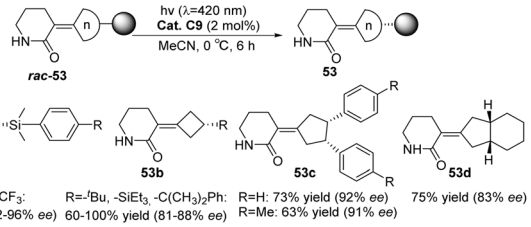

Scheme 24 Substrate range of photoderacemization of axially chiral olefins catalyzed by ketone **C9**.

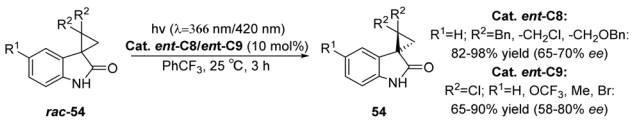

Scheme 25 Deracemization of 3-spirocyclopropyl 2-oxindoles.

substrate scope. Notably, this method enables the construction of a full-carbon stereocenter on cyclopropane, which holds significant potential for synthesizing chiral drugs analogous to cyclopropane derivatives.[85] Its good enantioselectivity is obtained through the synergistic effect of three mechanisms: (1) the difference in the binding constant with the chiral thiazolone, (2) the molecular distance of the enantiomer in the complex, and (3) the lifetime of the intermediate 1,3-diradical. According to NMR titration experiments, transient absorption spectroscopy measurements, and DFT calculations, the reaction mechanism was elucidated (Fig. 15). Due to steric hindrance, the interaction between **54** and the PS ***ent*-C9** to form **III** is thermodynamically unfavorable; however, the formation of **I** is more favorable and ultimately leads to the enrichment of enantiomer **54**.

In conclusion, the successful completion of catalytic deracemization in terms of PS units depends on the synergistic effect between chiral catalytic cycles and the photoenergy input cycle that overcomes thermodynamic and kinetic challenges. In addition, from the perspective of the chiral control unit,

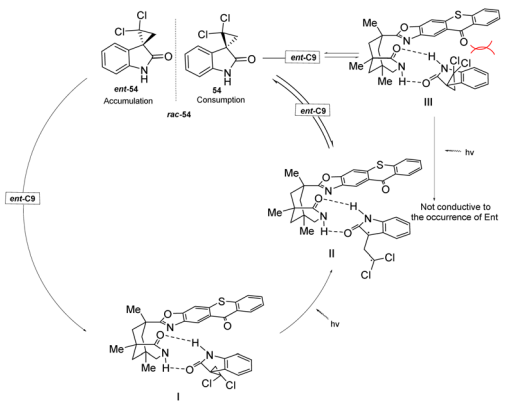

Fig. 15 Deracemization mechanism of 3-spirocyclopropyl 2-oxindoles catalyzed by ketone *ent*-C9.

whether a product with high enantioselectivity can be obtained depends on the difference between the spatial effect (such as steric hindrance) and the electronic effect (such as the degree of hydrogen bond binding and the influence of dispersion force) when the two enantiomers in the racemic substance are close to the catalyst. The spatial effect and the electronic effect lead to different degrees of association between the substrate and the photocatalyst, and the sensitization efficiency differ, ultimately affecting the enantioselectivity; therefore, the key points to consider when designing and selecting the catalyst for the photoderacemization reaction are the matching of the photosensitive unit with the reaction and the rational design of the chiral control unit.

4.3 Other asymmetric photocatalytic reactions

In recent years, thioxanthone-type catalysts have been utilized in various reactions, including the asymmetric [2 + 2] photocycloaddition reaction and racemization reaction mentioned earlier. Additionally, these catalysts have found application in other reactions, such as asymmetric electrophilic amination, asymmetric alkylation of aldehydes, and asymmetric α-hydroxylation reactions.

Masson *et al.* successfully synthesized a mono-substituted C1-symmetric photocatalyst **C14** by combining phosphoric acid and thioxanthone (Scheme 26).[71] The mono-substituted C1-symmetric photocatalyst exhibited superior catalytic efficiency compared with the corresponding C2-symmetric photocatalyst. Using catalyst **C14**, enecarbamate and azodicarboxylate were employed as starting materials for the reaction, which was conducted in two distinct steps. In the initial step, the nucleophilic enecarbamate reacted with the electrophilic azodicarboxylate to yield an imine, subsequently reacting with ethanethiol to form α-carbamoyl sulfide **I**. In the subsequent step, pyrazole was introduced, and the reaction was subjected to irradiation with blue light (λ = 420–510 nm). This led to the formation of imine **II**, which underwent a diastereothermal reaction with pyrazole to produce the ultimate product. The ee value achieved ranged from 95% to 99%.

The asymmetric electrophilic amination of α-unsubstituted enecarbamates was observed under 10 mol% catalyst **C15** upon irradiation with 405 nm. This reaction yielded chiral 1,2-diamides. The performance of catalyst **C15** was found to be satisfactory,[72] with only a minor disparity compared with catalyst **C14**.[71] This suggests that modifying the 3′-position substituents of the C1 symmetrical thioxanthone catalyst does not play a crucial role in determining the ee value of the substrate. In order to verify the universality of the results obtained by catalyst **C15**, several 1-(hetero)aryl-1,2-diamines were synthesized by changing the pyrazole ligand (Scheme 27). Good yield and enantioselectivity were obtained.

Alemán *et al.* successfully synthesized a novel catalyst, designated as catalyst **C16**, derived from thioxanthone through a two-step synthesis involving imidazolidinone and thioxanthone. This particular structure exhibits a convenient spatial property that can be readily adjusted. Notably, the catalyst

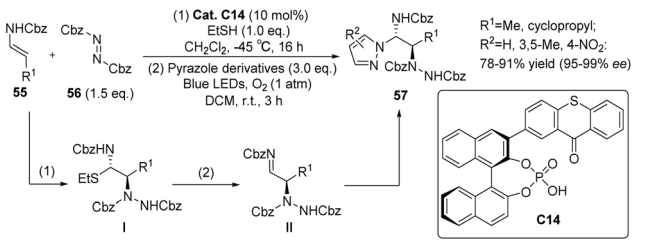

Scheme 26 Catalyst **C14** as photocatalyst enantioselective synthesis of 1,2-diamine.

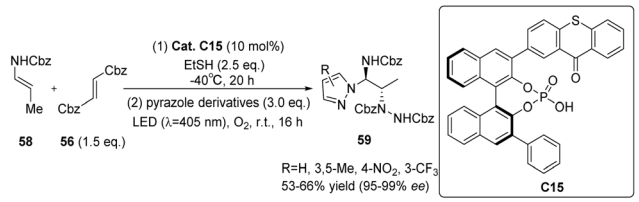

Scheme 27 Asymmetric electrophilic amination of enecarbamates catalyzed by ketone **C15**.

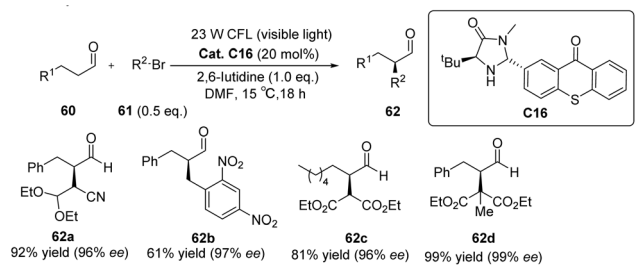

Scheme 28 Asymmetric alkylation of aldehydes catalyzed by ketone **C16**.

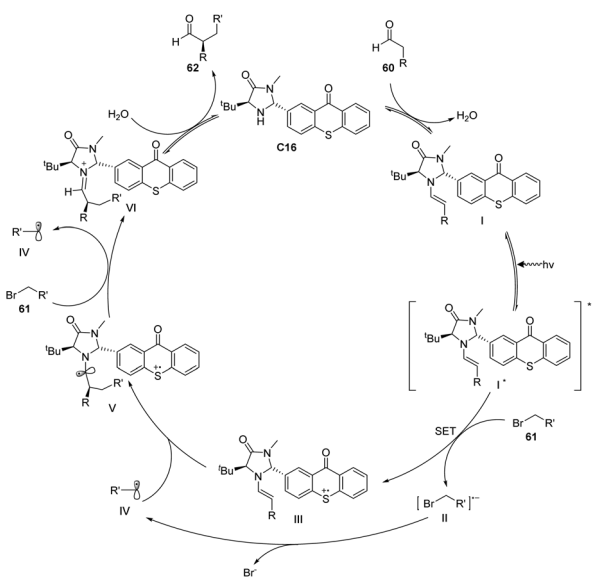

Fig. 16 Mechanism of asymmetric alkylation of aldehydes catalyzed by ketone **C16**.

demonstrates remarkable enantioselectivity and yield in the alkylation reaction of aldehydes, as depicted in Scheme 28.[73] The reaction mechanism is elucidated in Fig. 16. The thioxanthone of intermediate **I** is excited by light to produce the excited ketone **I***. Thioxanthone can promote the single electron transfer process (SET). The excited intermediate **I*** is used as a free radical chain initiator to reduce the bromoalkane derivative **61** through one SET, generating a free radical anion **II** and an enamine cation **III**. The bromine anion is left behind to produce free radical **IV** that reacts with the enamino cation intermediate **III** to produce α-amino radical **V**. Further, **VI** is obtained, and product **62** is obtained by hydrolysis, along with the chiral imidazolidinone–thioxanthone catalyst **C16**. The highlight of this work is the combination of photoredox catalysis and organic catalysis to achieve the asymmetric alkylation of aldehydes.

Xiao *et al.* designed a bifunctional catalyst that differs from Bach and developed a new photocatalyst, **C17**, by grafting the thioxanthone motif to the chiral BOX ligand.[74] The ground state of the thioxanthone component absorbs visible light and triplet state and then sensitizes the nonreactive triplet state of molecular oxygen ($^3O_2$) to produce the reactive singlet state of molecular oxygen ($^1O_2$). The chiral metal complexes derived from the BOX component activate the β-keto carbonyl group, thus controlling the selective formation of C–O bonds in the reaction. The ligand complexed with Ni (acac)$_2$ to catalyze the asymmetric α-hydroxylation of β-ketoesters to obtain products with high yields and ee values (Scheme 29). It should be noted that the catalyst does not directly act on the substrate but rather links the metal complex to the PS. The metal complex then activates the substrate while also controlling the chirality. In this context, the PS does not engage in direct activation of the substrate through energy or electron transfer. Instead, it indirectly sensitizes oxygen, inducing its transition from a nonreactive triplet state to a reactive singlet state, thus enabling oxygen's involvement in the reaction. Consequently, the successful achievement of the asymmetric aerobic oxidation of β-ketoesters and β-ketoamides was realized through visible light-induced metal photocatalysis, resulting in the production of α-hydroxy-β-dicarbonyl products. A possible stereoinduction model (Fig. 17) is proposed that assumes that the adamantyl

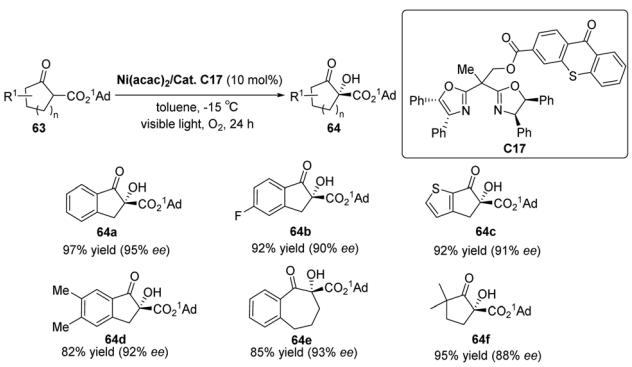

Scheme 29 Asymmetric α-hydroxylation of β-ketoesters catalyzed by the complexation of ketone **C17** with Ni (acac)$_2$ (^{1}Ad = 1-adamantyl).

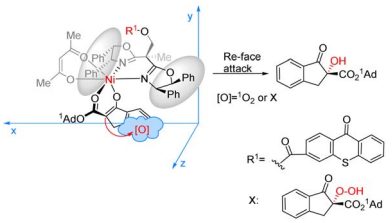

Fig. 17 Stereoinduction model of asymmetric α-hydroxylation catalyzed by complexation of ketone **C17** with Ni (acac)$_2$.

group (^{1}Ad–) is positioned far away from the chiral ligand to avoid steric hindrance. The *si*-face of the β-ketoester formed by the enol is obstructed by the phenyl group behind it; therefore, favorably, the oxidant attack from the *Re*-face activates $^1O_2$ or peroxide X, resulting in an R configuration for the hydroxylated product.

The aforementioned diverse reaction studies demonstrate the continued efficacy of bifunctional ketone catalysts incorporating sensitization and chiral control units in other asymmetric photoreactions, with ample potential for further exploration across various reaction types. Consequently, their future utilization in additional photochemical reactions is anticipated; however, the prerequisite for applying this type of catalyst to other reactions is the presence of a chiral control site in the substrate and a suitable reaction that can be initiated by the ketone PS unit, so that the ketone PS unit and chiral control unit can be reasonably designed according to the structure of the substrate to synthesize the required new ketone catalyst.

5. Summary and prospect

In the past decade, chiral ketone catalysts have shown great potential in the field of asymmetric catalysis. Chiral aromatic ketone catalysts exhibit high triplet energies and long triplet lifetimes, making them excellent PS units. These catalysts have become a powerful tool for asymmetric photocatalytic reactions; however, there is still room for future development in this field: (1) the modular formation of all-carbon quaternary stereocenters and multiple stereocenters remains a daunting challenge. (2) From the perspective of the PS unit of the catalyst, introducing various chiral skeletons to modify the chiral aromatic ketone photosensitive unit has shown limited effects. This limitation arises because the chiral aromatic ketone photosensitive unit itself may encounter issues such as mismatched redox potential or insufficient triplet energy. Furthermore, from the perspective of the chiral control unit of the catalyst, the chiral skeleton form is relatively simple. As a result, it can only exhibit an asymmetric catalytic role in specific substrates capable of forming hydrogen bonds, thus restricting its applicability to certain types of reactions.

In order to address the aforementioned issues, the future focus of development may lie in the design of new ketone catalysts. First, when designing the PS unit of the ketone catalyst, considering its match with the required light energy for the reaction is necessary, and this structure should be able to

complete the catalytic cycle through processes such as *ent*, HAT, or SET, which are decisive factors for initiating photosensitive reactions. Furthermore, obtaining a single chiral compound relies on an appropriate chiral skeleton. The design of a new chiral control unit can be achieved through various forces such as spatial effects, conjugation effects, induction effects, π–π stacking interactions, van der Waals forces, and hydrogen bonding. By combining different ketone PS units and chiral control units in diverse ways, it is possible to expand their application to more types of asymmetric photochemical reactions in the future. In summary, the application of ketone catalysts in [2 + 2] photocycloaddition reactions, deracemization reactions, photochemical rearrangement reactions, asymmetric electrophilic amination reactions, and the asymmetric alkylation of aldehydes were reviewed. The structural characteristics of these catalysts, the mechanism of catalytic reaction, and their advantages and disadvantages are discussed. It is hoped that it can provide the references for developing more applicable asymmetric catalytic methodologies in the future.

Data availability

Data availability is not applicable to this article as no new data were created or analyzed in this review. The findings presented in this review are based on previously published works cited in the reference list.

Author contributions

B. J. B. collected the literature and wrote the manuscripts L. Y. and L. X. Q. revised the manuscript. Q. Z. and W. H. supervised the work and revised the manuscript.

Conflicts of interest

The authors declare no conflict of interest.

Acknowledgements

This research is supported by the Xijing Innovation Institute Joint Fund (No. LHJJ2023-YX04), the Qin Chuangyuan's Team Building Project (No. 2022KXJ-101), the Science and Technology Program of Gansu Province (No. 23ZDFA003), the National Natural Science Foundation of China (No. 21272272), the Project of Research and Development of Key Technologies (No. 2023-YBGY-486), and the Natural Science Basic Research Program of Shaanxi (No. 2023-JC-QN-0149, 2023-JC-QN-0868).

References

1 I. Triandafillidi, D. I. Tzaras and C. G. Kokotos, *ChemCatChem*, 2018, **10**, 2521–2535.
2 L. D'Accolti, C. Annese and C. Fusco, *Chemistry*, 2019, **25**, 12003–12017.
3 N. Hoffmann, *Photochem. Photobiol. Sci.*, 2021, **20**, 1657–1674.
4 A. Antenucci, S. Dughera and P. Renzi, *ChemSusChem*, 2021, **14**, 2785–2853.
5 T. H. El-Assaad, J. Zhu, A. Sebastian, D. V. McGrath, I. Neogi and K. N. Parida, *Org. Chem. Front.*, 2022, **9**, 5675–5725.
6 M. J. Genzink, J. B. Kidd, W. B. Swords and T. P. Yoon, *Chem. Rev.*, 2022, **122**, 1654–1716.
7 J. Wang, X. Lv and Z. Jiang, *Chem.–Eur. J.*, 2023, **29**, e202204029.
8 Y. Shi, *Acc. Chem. Res.*, 2004, **37**, 488–496.
9 D. Yang, *Acc. Chem. Res.*, 2004, **37**, 497–505.
10 O. A. Wong and Y. Shi, *Chem. Rev.*, 2008, **108**, 3958–3987.
11 R. L. Davis, J. Stiller, T. Naicker, H. Jiang and K. A. Jørgensen, *Angew. Chem., Int. Ed.*, 2014, **53**, 7406–7426.
12 Y. Zhu, Q. Wang, R. G. Cornwall and Y. Shi, *Chem. Rev.*, 2014, **114**, 8199–8256.
13 Y. Tu, Z.-X. Wang and Y. Shi, *J. Am. Chem. Soc.*, 1996, **118**, 9806–9807.
14 Z. Xiong and E. J. Corey, *J. Am. Chem. Soc.*, 2000, **122**, 4831–4832.
15 D. W. Hoard, E. D. Moher, M. J. Martinelli and B. H. Norman, *Org. Lett.*, 2002, **4**, 1813–1815.
16 C. M. Adams, I. Ghosh and Y. Kishi, *Org. Lett.*, 2004, **6**, 4723–4726.
17 Y. Morimoto, Y. Nishikawa and M. Takaishi, *J. Am. Chem. Soc.*, 2005, **127**, 5806–5807.
18 A. B. Smith, S. P. Walsh, M. Frohn and M. O. Duffey, *Org. Lett.*, 2005, **7**, 139–142.
19 F. Lecornué, R. Paugam and J. Ollivier, *Eur. J. Org Chem.*, 2005, **2005**, 2589–2598.
20 D. F. Taber and Y. He, *J. Org. Chem.*, 2005, **70**, 7711–7714.
21 J. Bian, M. Van Wingerden and J. M. Ready, *J. Am. Chem. Soc.*, 2006, **128**, 7428–7429.
22 R. M. Kanada, D. Itoh, M. Nagai, J. Niijima, N. Asai, Y. Mizui, S. Abe and Y. Kotake, *Angew. Chem., Int. Ed.*, 2007, **46**, 4350–4355.
23 A. R. Van Dyke and T. F. Jamison, *Angew Chem. Int. Ed. Engl.*, 2009, **48**, 4430–4432.
24 M. Yu and B. B. Snider, *Org. Lett.*, 2009, **11**, 1031–1032.
25 T. J. Harrison, S. Ho and J. L. Leighton, *J. Am. Chem. Soc.*, 2011, **133**, 7308–7311.
26 D. J. Clausen, S. Wan and P. E. Floreancig, *Angew Chem. Int. Ed. Engl.*, 2011, **50**, 5178–5181.
27 P. Yang, P.-F. Li, J. Qu and L.-F. Tang, *Org. Lett.*, 2012, **14**, 3932–3935.
28 A. K. Ghosh and D. D. Anderson, *Org. Lett.*, 2012, **14**, 4730–4733.
29 V. P. Kumar and S. Chandrasekhar, *Org. Lett.*, 2013, **15**, 3610–3613.
30 C. An, J. A. Jurica, S. P. Walsh, A. T. Hoye and A. B. Smith, *J. Org. Chem.*, 2013, **78**, 4278–4296.
31 T. Kodama, S. Aoki, S. Kikuchi, T. Matsuo, Y. Tachi, K. Nishikawa and Y. Morimoto, *Tetrahedron Lett.*, 2013, **54**, 5647–5649.
32 D. J. Mack and J. T. Njardarson, *Angew. Chem., Int. Ed.*, 2013, **52**, 1543–1547.
33 Y. Morimoto, E. Takeuchi, H. Kambara, T. Kodama, Y. Tachi and K. Nishikawa, *Org. Lett.*, 2013, **15**, 2966–2969.

34 J. Rodríguez-López, F. Pinacho Crisóstomo, N. Ortega, M. López-Rodríguez, V. S. Martín and T. Martín, *Angew Chem. Int. Ed. Engl.*, 2013, **52**, 3659–3662.
35 S. Sittihan and T. F. Jamison, *J. Am. Chem. Soc.*, 2019, **141**, 11239–11244.
36 D. Rhoades, A. L. Rheingold, B. W. O'Malley and J. Wang, *J. Am. Chem. Soc.*, 2021, **143**, 4915–4920.
37 T. Ohyoshi, H. Iizumi, S. Hosono, H. Tano and H. Kigoshi, *Org. Lett.*, 2023, **25**, 4725–4729.
38 Z. Tan, X. Ju, H. Wu, W. Dong, J. C. Leung, X. Hou, H. Lee, A. Granger, J. M. Paolillo, S. V. DiMeo, C. Chen, L. Wu, J. C. Lorenz, M. Sarvestani, F. Buono, R. Frutos, T. G. Tampone, X. Huang, G. Zhang, Y. Wang, E. Spinelli, Z. Lei and J. J. Song, *Org. Process Res. Dev.*, 2024, **28**, 78–91.
39 P. Jiang, S. Wu, G. Wang, S. Xiang and B. Tan, *Angew. Chem., Int. Ed.*, 2023, **40**, e202309272.
40 C. Michelin and N. Hoffmann, *ACS Catal.*, 2018, **8**, 12046–12055.
41 J. Zhao, W. Wu, J. Sun and S. Guo, *Chem. Soc. Rev.*, 2013, **42**, 5323–5351.
42 D. E. Damschen, C. D. Merritt, D. L. Perry, G. W. Scott and L. D. Talley, *J. Phys. Chem.*, 1978, **82**, 2268–2272.
43 C. Ouannès, R. Beugelmans and G. Roussi, *J. Am. Chem. Soc.*, 1973, **95**, 8472–8474.
44 M. Demuth, P. R. Raghavan, C. Carter, K. Nakano and K. Schaffner, *Helv. Chim. Acta*, 1980, **63**, 2434–2439.
45 H. Rau and M. Hörmann, *J. Photochem.*, 1981, **16**, 231–247.
46 A. Bauer, F. Westkämper, S. Grimme and T. Bach, *Nature*, 2005, **436**, 1139–1140.
47 R. Sebesta, *Beilstein J. Org. Chem.*, 2022, **18**, 240–242.
48 J. Großkopf, T. Kratz, T. Rigotti and T. Bach, *Chem. Rev.*, 2022, **122**, 1626–1653.
49 M. J. Genzink, J. B. Kidd, W. B. Swords and T. P. Yoon, *Chem. Rev.*, 2022, **122**, 1654–1716.
50 D. F. Cauble, V. Lynch and M. J. Krische, *J. Org. Chem.*, 2003, **68**, 15–21.
51 J. Großkopf, M. Plaza, A. Seitz, S. Breitenlechner, G. Storch and T. Bach, *J. Am. Chem. Soc.*, 2021, **143**, 21241–21245.
52 J. Großkopf, A. A. Heidecker and T. Bach, *Angew. Chem., Int. Ed.*, 2023, **62**, e202305274.
53 C. Müller, A. Bauer, M. M. Maturi, M. C. Cuquerella, M. A. Miranda and T. Bach, *J. Am. Chem. Soc.*, 2011, **133**, 16689–16697.
54 M. M. Maturi, A. Pöthig and T. Bach, *Aust. J. Chem.*, 2015, **68**, 1682–1692.
55 L. Wimberger, T. Kratz and T. Bach, *Synthesis*, 2019, **51**, 4417–4424.
56 M. M. Maturi and T. Bach, *Angew. Chem., Int. Ed.*, 2014, **53**, 7661–7664.
57 R. Alonso and T. Bach, *Angew. Chem., Int. Ed.*, 2014, **53**, 4368–4371.
58 X. Li, C. Jandl and T. Bach, *Org. Lett.*, 2020, **22**, 3618–3622.
59 A. Tröster, R. Alonso, A. Bauer and T. Bach, *J. Am. Chem. Soc.*, 2016, **138**, 7808–7811.
60 T. Kratz, P. Steinbach, S. Breitenlechner, G. Storch, C. Bannwarth and T. Bach, *J. Am. Chem. Soc.*, 2022, **144**, 10133–10138.
61 A. Tröster, A. Bauer, C. Jandl and T. Bach, *Angew. Chem., Int. Ed.*, 2019, **58**, 3538–3541.
62 X. Li, J. Großkopf, C. Jandl and T. Bach, *Angew. Chem., Int. Ed.*, 2021, **60**, 2684–2688.
63 A. Hölzl-Hobmeier, A. Bauer, A. V. Silva, S. M. Huber, C. Bannwarth and T. Bach, *Nature*, 2018, **564**, 240–243.
64 M. Plaza, C. Jandl and T. Bach, *Angew. Chem., Int. Ed.*, 2020, **59**, 12785–12788.
65 M. Plaza, J. Großkopf, S. Breitenlechner, C. Bannwarth and T. Bach, *J. Am. Chem. Soc.*, 2021, **143**, 11209–11217.
66 F. Mayr, L.-M. Mohr, E. Rodriguez and T. Bach, *Synthesis*, 2017, **49**, 5238–5250.
67 F. Pecho, Y. Zou, J. Gramüller, T. Mori, S. M. Huber, A. Bauer, R. M. Gschwind and T. Bach, *Chem.–Eur. J.*, 2020, **26**, 5190–5194.
68 F. Pecho, Y. Sempere, J. Gramüller, F. M. Hörmann, R. M. Gschwind and T. Bach, *J. Am. Chem. Soc.*, 2021, **143**, 9350–9354.
69 R. Takagi and T. Tanimoto, *Org. Biomol. Chem.*, 2022, **20**, 3940–3947.
70 S. C. Huo, R. R. Indurmuddam, B.-C. Hong, C.-F. Lu and S.-Y. Chien, *Org. Biomol. Chem.*, 2023, **21**, 9330–9336.
71 J. Lyu, A. Claraz, M. R. Vitale, C. Allain and G. Masson, *J. Org. Chem.*, 2020, **85**, 12843–12855.
72 J. Lyu, M. Leone, A. Claraz, C. Allain, L. Neuville and G. Masson, *RSC Adv.*, 2021, **11**, 36663–36669.
73 T. Rigotti, A. Casado-Sánchez, S. Cabrera, R. Pérez-Ruiz, M. Liras, V. A. de la Peña O'Shea and J. Alemán, *ACS Catal.*, 2018, **8**, 5928–5940.
74 W. Ding, L.-Q. Lu, Q.-Q. Zhou, Y. Wei, J.-R. Chen and W.-J. Xiao, *J. Am. Chem. Soc.*, 2017, **139**, 63–66.
75 W. H. Pirkle and D. S. Reno, *J. Am. Chem. Soc.*, 1987, **109**, 7189–7190.
76 R. J. Kutta, J. Großkopf, N. Van Staalduinen, A. Seitz, P. Pracht, S. Breitenlechner, C. Bannwarth, P. Nuernberger and T. Bach, *J. Am. Chem. Soc.*, 2023, **145**, 2354–2363.
77 C. Müller, A. Bauer and T. Bach, *Angew. Chem., Int. Ed.*, 2009, **48**, 6640–6642.
78 A. Bakowski, M. Dressel, A. Bauer and T. Bach, *Org. Biomol. Chem.*, 2011, **9**, 3516–3529.
79 M. M. Maturi, M. Wenninger, R. Alonso, A. Bauer, A. Pöthig, E. Riedle and T. Bach, *Chem.–Eur. J.*, 2013, **19**, 7461–7472.
80 L. Wang, Z. Li, L. Lu and W. Zhang, *Tetrahedron*, 2012, **68**, 1483–1491.
81 E. C. Lathioor and W. J. Leigh, *Photochem. Photobiol.*, 2006, **82**, 291–300.
82 Z.-L. Xia, Q.-F. Xu-Xu, C. Zheng and S.-L. You, *Chem. Soc. Rev.*, 2020, **49**, 286–300.
83 T. Akiyama, J. Itoh, K. Yokota and K. Fuchibe, *Angew. Chem., Int. Ed.*, 2004, **43**, 1566–1568.
84 K. Yuan, P. Wang, H.-X. Li, Y.-Z. Liu and L.-L. Lv, *Org. Chem. Front.*, 2020, **7**, 3656–3663.
85 X. Li, R. J. Kutta, C. Jandl, A. Bauer, P. Nuernberger and T. Bach, *Angew. Chem., Int. Ed.*, 2020, **59**, 21640–21647.